Supporting Information

Electrodeposited Co-doped $Mn(OH)_2$ for Exploring the Electrochemical Conversion of Phenol to *para*-Benzoquinone

Lingrui Shi, Xinyue Gu, Xiaohan Liu, Xiaotong Jin, Zhiping Xiong,* Rui Cao* and Wei Zhang*

Key Laboratory of Applied Surface and Colloid Chemistry, Ministry of Education School of Chemistry and Chemical Engineering, Shaanxi Normal University, Xi'an 710119, China

*Correspondence E-mails: xiongzp@snnu.edu.cn; ruicao@snnu.edu.cn; zw@snnu.edu.cn

Experimental Section

Chemicals

Phenol (C_6H_6O, 99.0%), *p*-benzoquinone ($C_6H_5O_2$, 98.0%), manganese nitrate ($Mn(NO_3)_2·4H_2O$, 98.0%), cobalt nitrate ($Co(NO_3)_2·6H_2O$, 98.0%), sodium sulfate (Na_2SO_4, 99.0%) were purchased from Energy Chemical Co., Ltd. Hydrochloric acid (HCl, 36.0–38.0%), sulfuric acid (H_2SO_4, 95.0–98.0%) were obtained from Sinopharm Chemical Reagent Co., Ltd. Ultrapure water (18 MΩ·cm at 25 °C) from a Millipore water purification system was used throughout the experiments. All chemicals were used without further purification.

Preparation of electrodes

Preparation of the etched NF

To prepare the etched NF, blank NF was firstly sonicated in 2.0 M HCl, water and ethanol to remove surface pollutants and oxides. Then, one piece of the pretreated NF ($1×1$ cm^2) was used as the working electrode for controlled potential electrolysis at 0.08 V vs. Ag/AgCl in 0.5 M H_2SO_4 for 300 s; graphite rod was the counter electrode. The obtained etched NF was collected by washing with water and ethanol for several times and was stocked in ethanol for subsequent uses.

Preparation of Co-$Mn(OH)_2$/NF electrode

The Co-$Mn(OH)_2$/NF electrode was fabricated via a one-step electrodeposition method using a three-electrode system, by applying a potential of −1.2 V vs. Ag/AgCl for 100 s in a 50 mL electrolyte containing 50 mM $Mn(NO_3)_2·4H_2O$ and 0.5 mM $Co(NO_3)_2·6H_2O$, using etched NF, Ag/AgCl, and a Pt sheet as the working, reference,

and counter electrodes, respectively. The electrode preparation was conducted under neutral pH conditions. Finally, the as-obtained Co-$Mn(OH)_2$/NF electrode was rinsed with ultrapure water. Other electrodes were prepared following a similar procedure in electrolyte solutions containing different metal salts.

Physical characterizations

Field-emission scanning electron microscopy (FESEM) images were obtained by a Hitachi SU8820 cold-emission field emission scanning electron microscope with 5 kV accelerating voltage. Energy-dispersive X-ray (EDX) analysis and elemental mapping were conducted using an AMETEK Materials Analysis EDX equipped on the SEM. The crystal structures were determined using X-ray diffraction (XRD, a Rigaku D/Max2550VB+/PC X-ray diffractometer with Cu Kα radiation source). The amounts of Mn and Co deposited on the electrode was quantified by inductively coupled plasma optical emission spectroscopy (ICP-OES). Transmission electron microscopy (TEM) images were taken on a JEOL JEM-2100F high-resolution transmission electron microscope (HR-TEM). High-angle annular dark-field scanning transmission electron microscope (HAADF–STEM) images were acquired on an FEI Tecnai G2 F2O field transmission electron microscope operated at 200 kV. X-ray photoelectron spectroscopy (XPS) analysis of the catalyst was conducted on a Kratos AXIS ULTRA XPS analyzer with monochromatized Al Kα (hν = 1486.6eV) X-ray source. Corrections of the XPS binding energy were carried out using C 1s peak at 284.8 eV. Raman spectra were carried out using a Lab RAM Odyssey in ViaReflex Raman spectrometer with an excitation wave length of 532nm. Transmission X-ray absorption fine structure (XAFS)

measurements were tested using a laboratory device (easyXAFS300+, easyXAFS LLC). Hydrophilic phenol solution property were measured by a video-based optical contact angle instrument (KRUSS-DSA100) with dropping the catalyst of the same loading amount onto the glass slide.

Electrochemical measurements

Unless otherwise specified, all ECO electrolysis experiments were carried out in a sealed H-type cell, separated by a Nafion 117 proton exchange membrane, using an electrochemical workstation (CHI 660E, Chenhua Co., Ltd, China). The as-prepared electrodes were used as the working electrodes, with a Ti sheet and saturated Ag/AgCl electrode used as the counter and reference electrodes, respectively. The effects of electrocatalytic oxidation potential (0.5–1.3 V) and electrolysis duration (1–5 h) on the ECO performance of phenol were systematically investigated. All subsequent ECO experiments employing different electrodes were conducted under the optimized electrolytic conditions with stirring at 400 rpm, and the results were presented as the mean and standard deviation derived from triplicate measurements or repeated experimental runs.

Other electrochemical measurements of the catalysts were performed on a CHI 660E electrochemical workstation at room temperature with a three-electrode system, where the as-prepared electrode (1 cm^2), Pt sheet, and saturated Ag/AgCl electrode served as the working, counter, and reference electrodes, respectively. 100 mM $NaSO_4$ was used as the electrolyte. The ECO of phenol of different electrodes was determined by linear sweep voltammetry (LSV) from 0 V to 1.5 V vs. Ag/AgCl at a scan rate of 5

mV/s. Electrochemical impedance spectroscopy (EIS) was employed over a frequency range of 100 kHz to 0.01 Hz with an amplitude of 5 mV. The electrochemically active surface areas (ECSA) were determined by measuring the electrical double-layer capacitance (C_{dl}) by cyclic voltammograms (CV) in the non-Faradaic potential region at scan rates from 20 to 120 mV/s. The C_{dl} stem from the slope of the plot of $\Delta J/2$ (half of the current density difference at the centered potential) against the scan rate. The long-term activity of electrodes was evaluated by chronopotentiometry measurements with a set anodic potential of 0.9 V (vs Ag/AgCl).

Analytic methods

The concentrations of phenol and *p*-BQ in solution were analyzed by a high-performance liquid chromatography (HPLC, Agilent 1260) equipped with a diode array detector (DAD) and a 120 EC-C18 column (3.0 ×250 mm). Samples (20 μL) were loaded on a BEH C18 column (250 mm × 3.0 mm i.d., 2.7 μm; Waters, Agilent) Specifically. The column temperature was maintained at 40 °C, with a mobile phase (A: 0.5% ammonium acetate, B: acetonitrile) at a flow rate of 0.5 mL/min. The mobile phase ratio of A/B was set to 50/50 and was held for 8 min.

The ECO performance of phenol, including conversion of phenol (equation 1) and yield of *p*-BQ (equation 2) were evaluated via the following equations. The Faradaic efficiency (F.E., equation 3) were calculated to evaluate the ECO activity of the system.

$$\text{Conversion of phenol (\%)} = \frac{\text{Phenol converted (mol)}}{\text{Phenol input (mol)}} \times 100\% \quad \text{(S1)}$$

$$\text{Yield of } p\text{-BQ (\%)} = \frac{p\text{-BQ produced (mol)}}{\text{Phenol input (mol)}} \times 100\% \quad \text{(S2)}$$

$$\text{F.E. (\%)} = \frac{4nF}{Q} \times 100\% \quad \text{(S3)}$$

where n is the generated amount of *p*-BQ (mol) and the conversion amount of phenol (mol). Since electrooxidation of phenol into *p*-BQ is our main research reaction, the influence of other reaction pathways on the FE was not considered. 4 is the corresponding number of electrons transferred (based on the 4-electron 4-proton reaction pathway), F is the Faraday constant (96485.3 C/mol) and Q (C) is the total charge transferred through the circuit.

Supplementary Figures

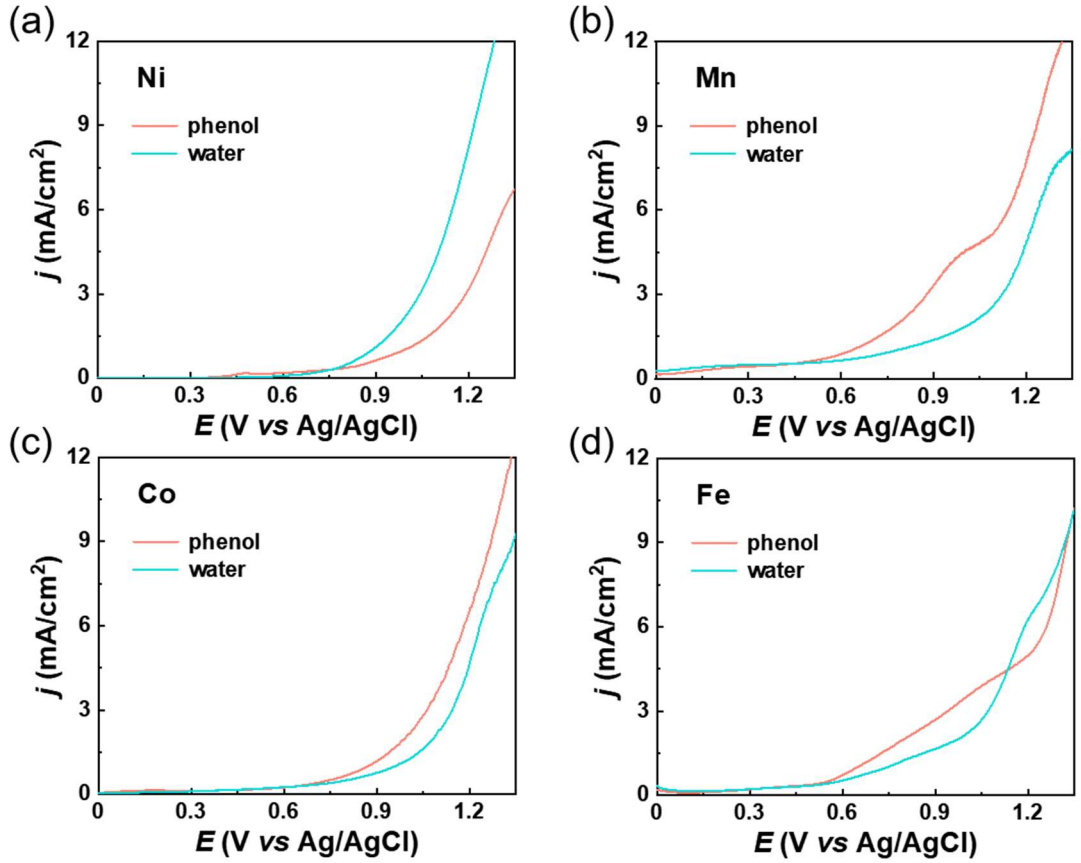

Figure S1. The electrocatalytic activity of the electrodes loaded with different transition metal hydroxides: (a) Ni, (b) Mn, (c) Co and (d) Fe in a 100 mM Na_2SO_4 electrolyte with (ECO) and without (OER) 10 mM phenol.

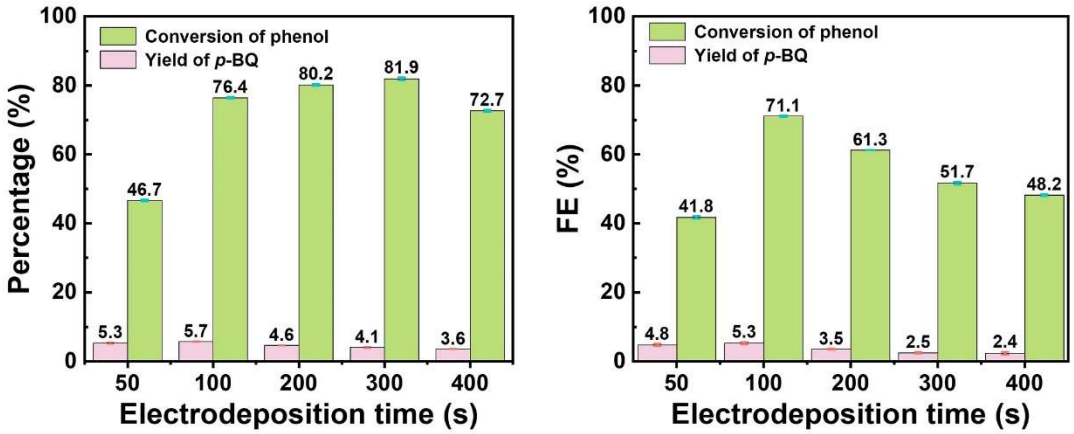

Figure S2. The optimization of the electrodeposition time for the preparation of $Mn(OH)_2$/NF electrodes. Experimental parameters for electrodeposition process: $Mn(NO_3)_2 \cdot 4H_2O$ at 50 mM, applied potential at −1.2 V, time at 100 s.

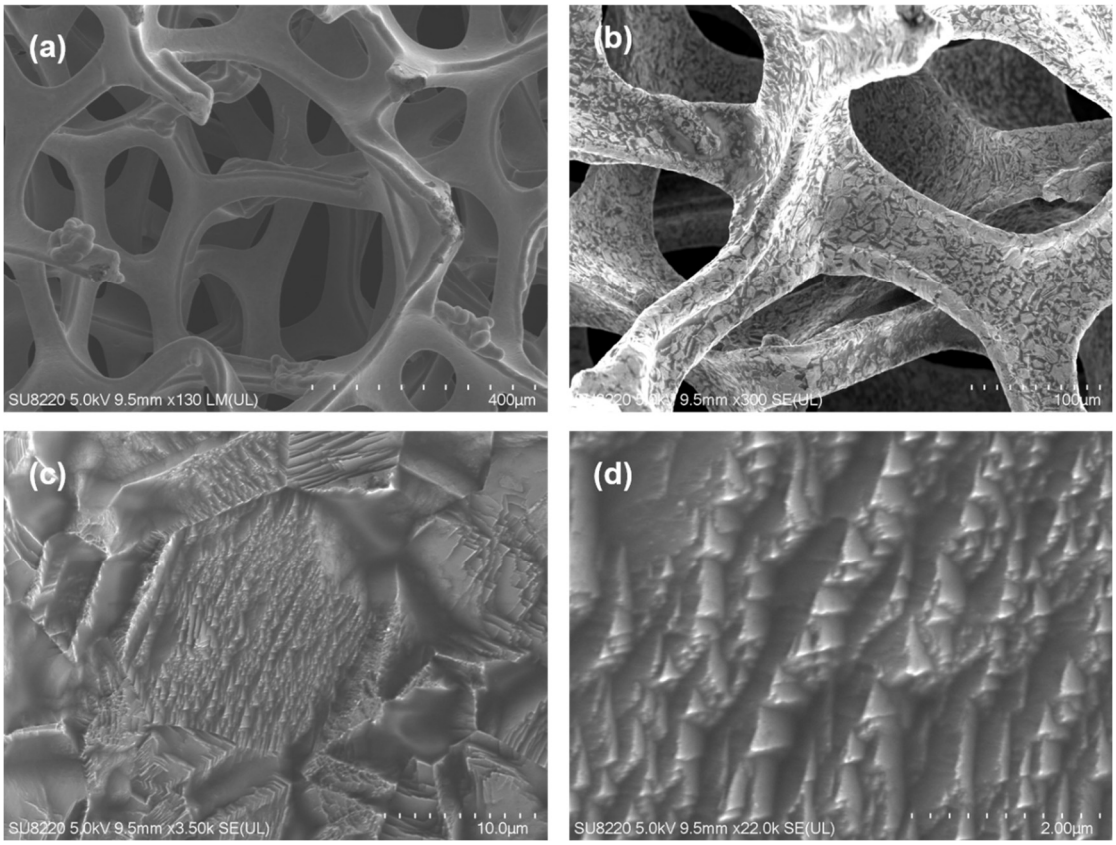

Figure S3. SEM images of (a) blank NF and (b-d) electrochemical etched NF.

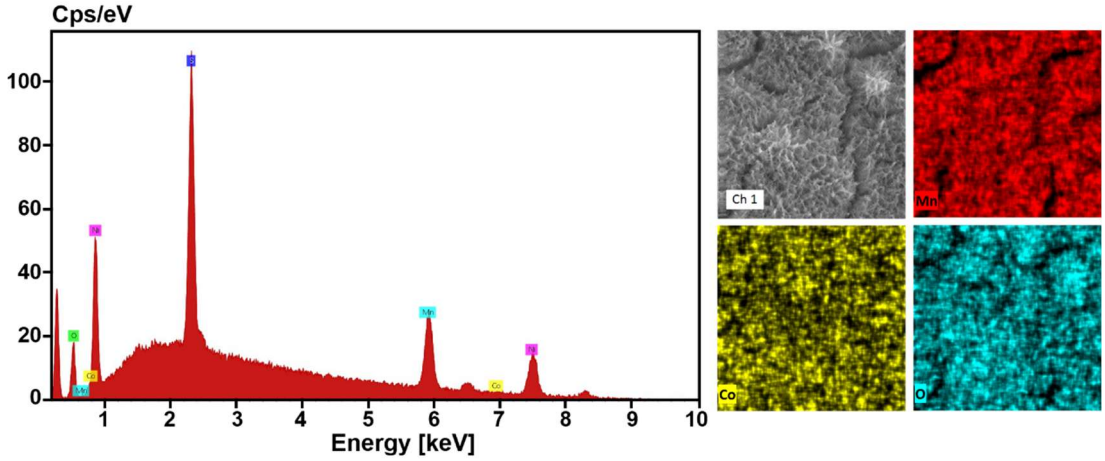

Figure S4. EDX spectrum and the corresponding elemental mapping images of the Co-$Mn(OH)_2$/NF.

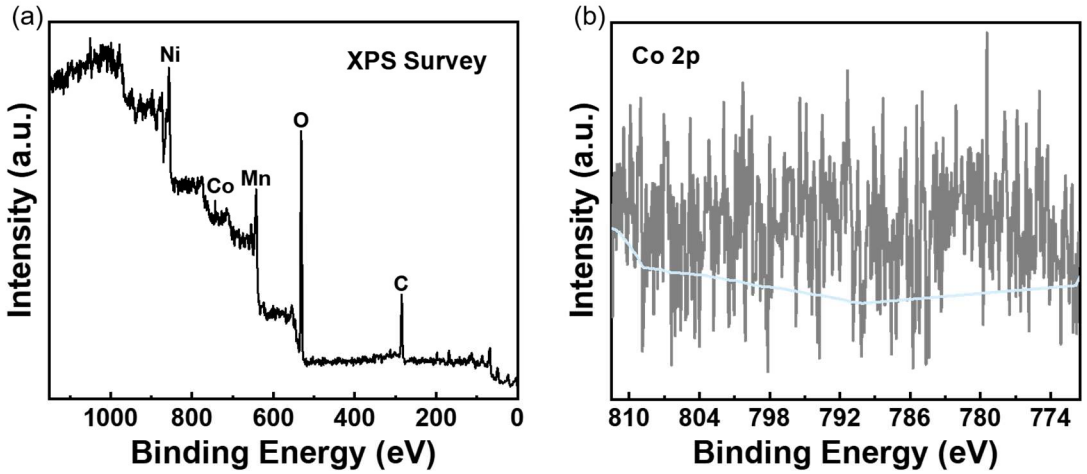

Figure S5. (a) XPS survey spectrum and (b) Co 2p spectrum of Co-Mn$(OH)_2$/NF.

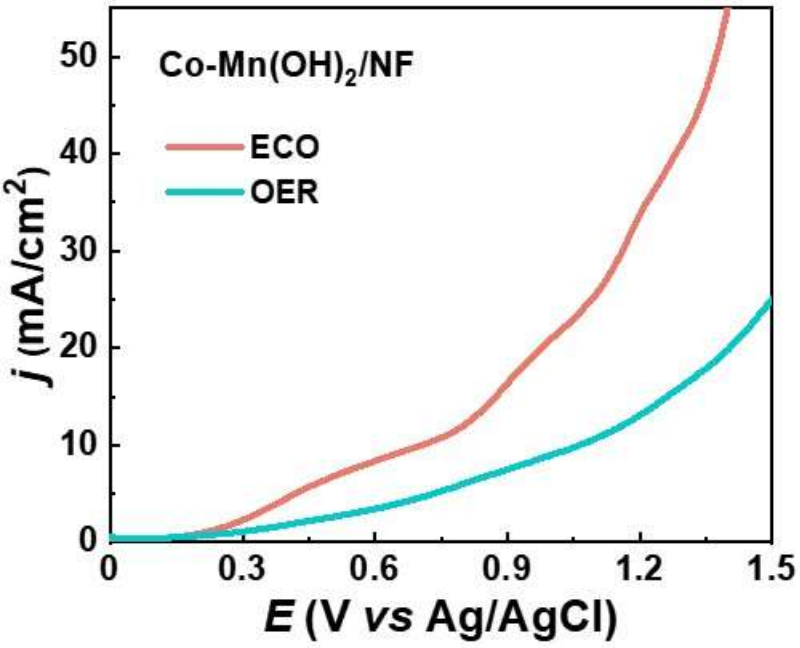

Figure S6. LSV curves of the Co-$Mn(OH)_2$/NF electrode in a Na_2SO_4 electrolyte with (ECO) and without (OER) 10 mM phenol.

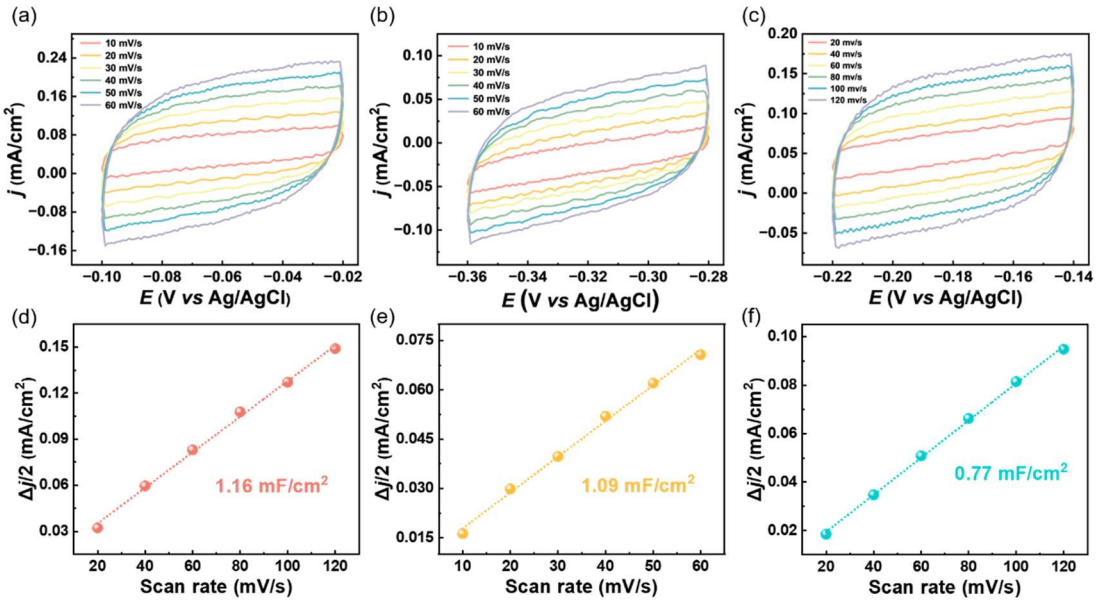

Figure S7. CV curves of (a) Co-$Mn(OH)_2$/NF, (b) $Mn(OH)_2$/NF, (c) etched NF at different scan rates in the non-Faradaic potential range. The double-layer capacitances (C_{dl}) of (d) Co-$Mn(OH)_2$/NF, (e) $Mn(OH)_2$/NF, (f) etched NF

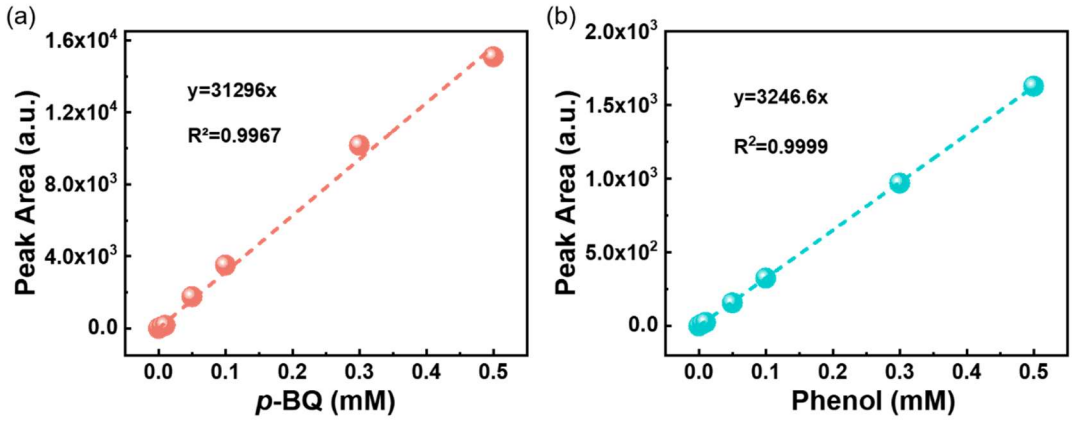

Figure S8. The standard curves for (a) *p*-BQ and (b) phenol obtained by HPLC.

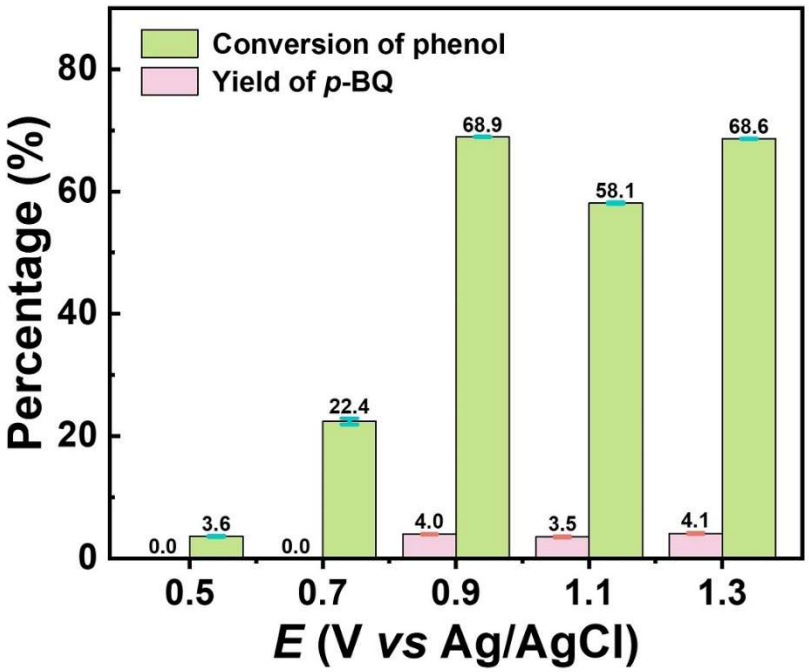

Figure S9. The ECO performance for the oxidation of phenol from the electrolysis of 3 h by the $Mn(OH)_2$/NF electrode at different potentials.

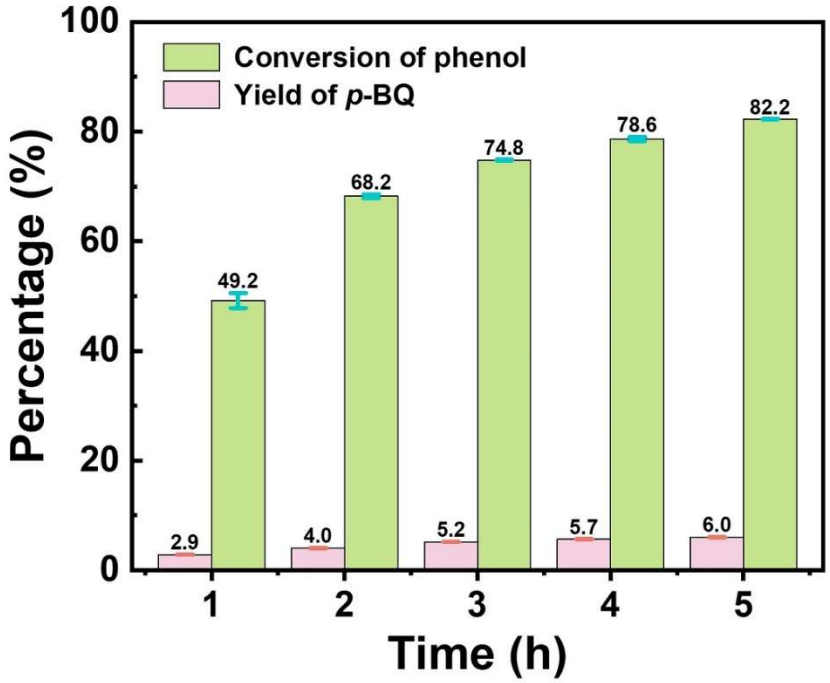

Figure S10. The ECO performance for the oxidation of phenol from the electrolysis of different times by the $Mn(OH)_2$/NF electrode at 0.9 V.

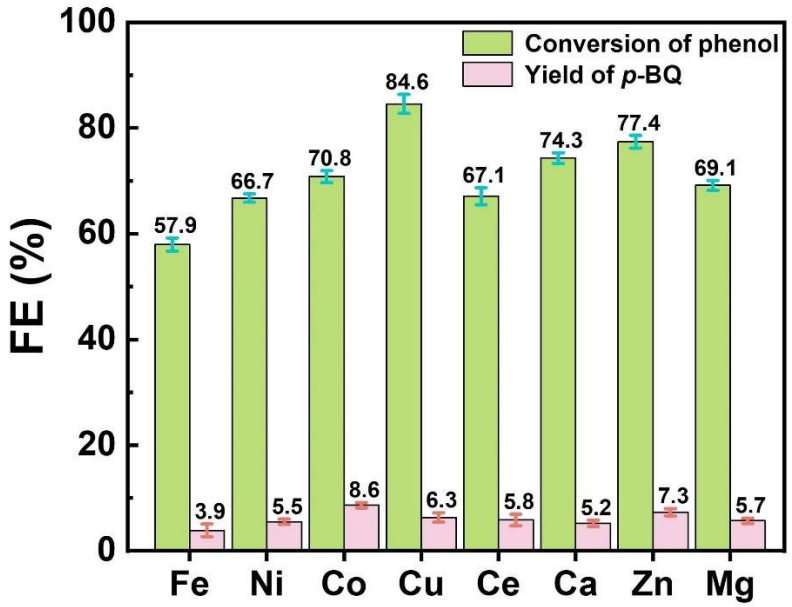

Figure S11. The ECO performance for the oxidation of phenol from the electrolysis of 2 h at 0.9 V by M-$Mn(OH)_2$/NF electrodes doped with different metals.

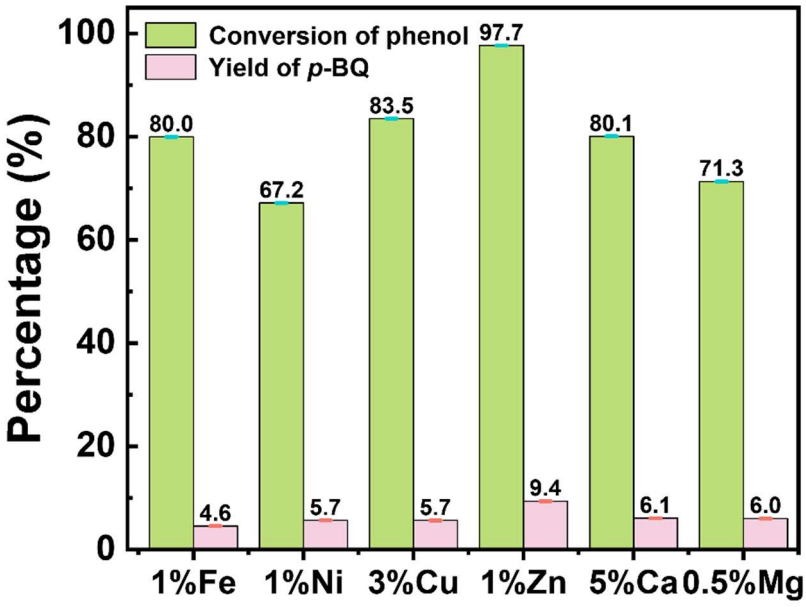

Figure S12. The ECO performance under the optimal doping ratios of different metals.

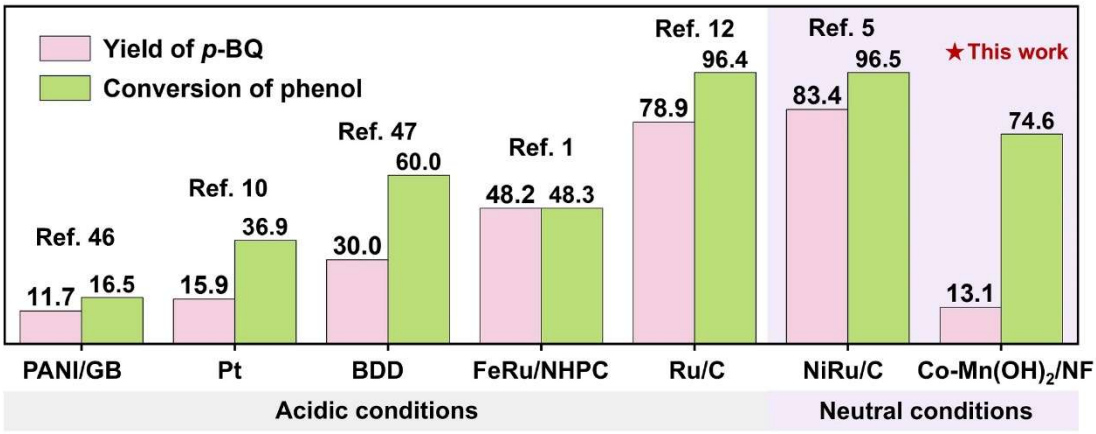

Figure S13. The ECO performance comparison of phenol conversion and *p*-BQ yield for Co-Mn(OH)$_2$/NF and those reported in the literature (references are provided in the manuscript).

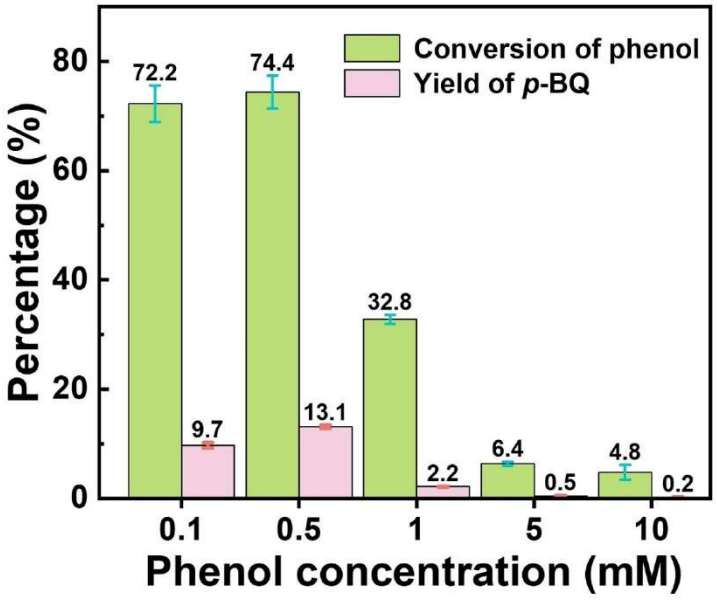

Figure S14. The ECO performance for the oxidation of phenol from the electrolysis of 2 h with varying concentrations of phenol by Co-$Mn(OH)_2$/NF electrode at 0.9 V.

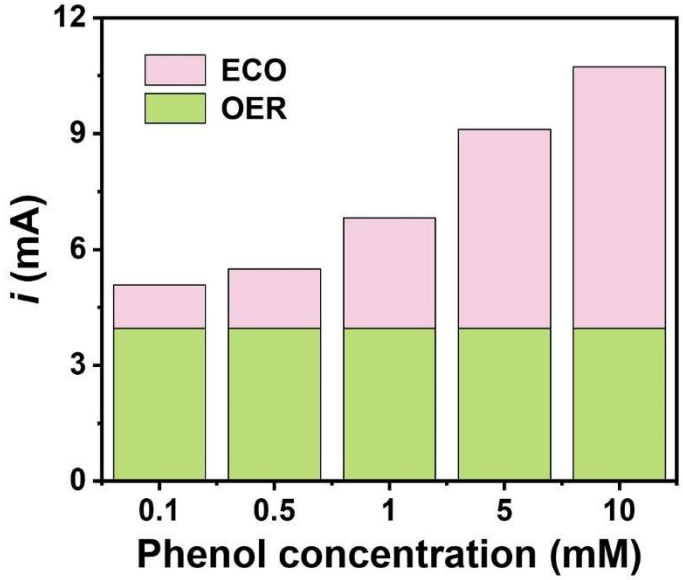

Figure S15. The current portion between ECO and OER under different phenol concentrations at 1.1 V.

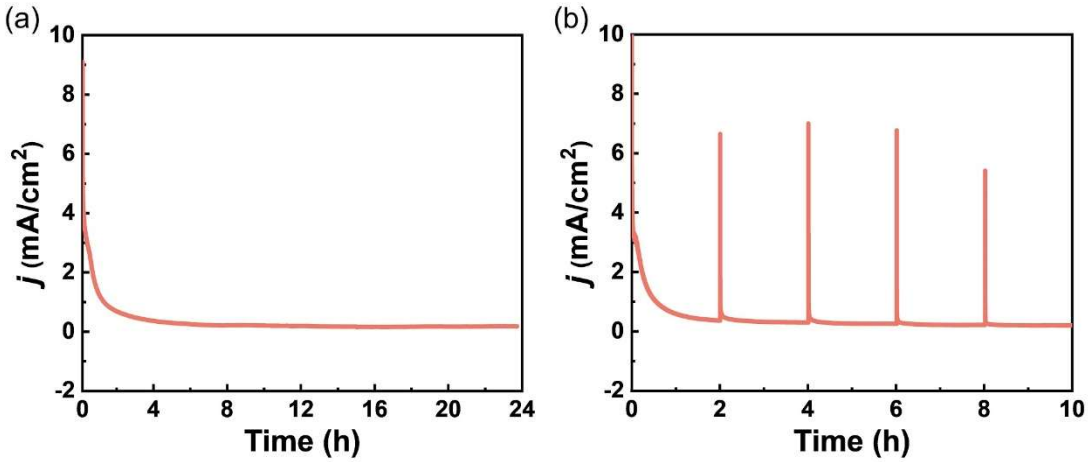

Figure S16. The ECO stability test of phenol oxidation by Co-$Mn(OH)_2$/NF at 0.9 V (a) without and (b) with refreshing electrolyte every 2 h.

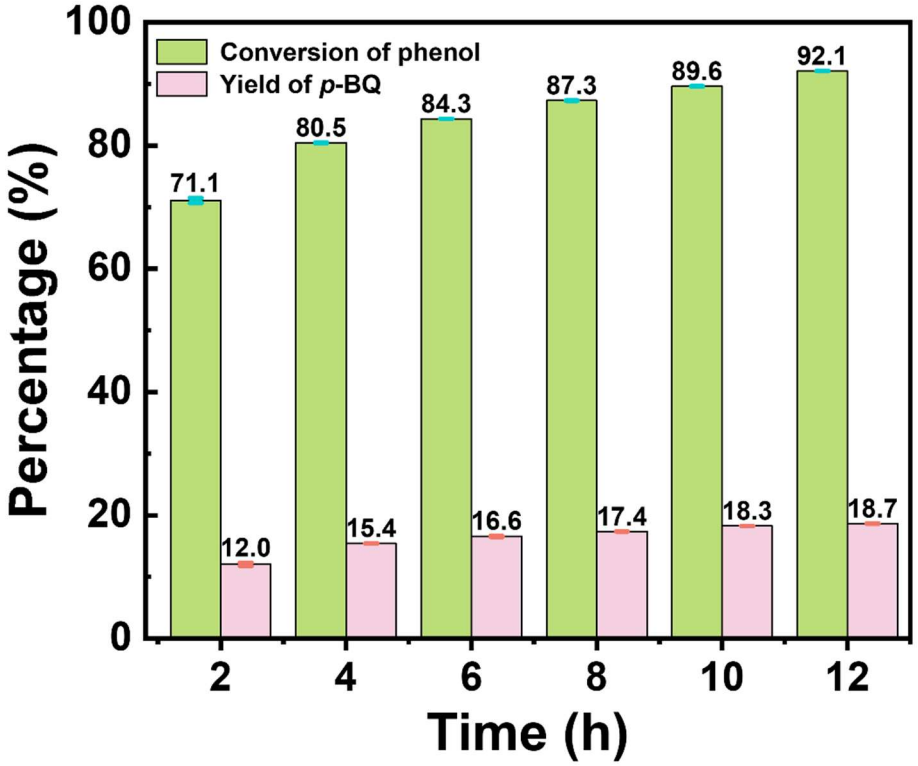

Figure S17. The ECO performance by the Co-$Mn(OH)_2$/NF electrode at 0.9 V during the 12h long-term measurements.

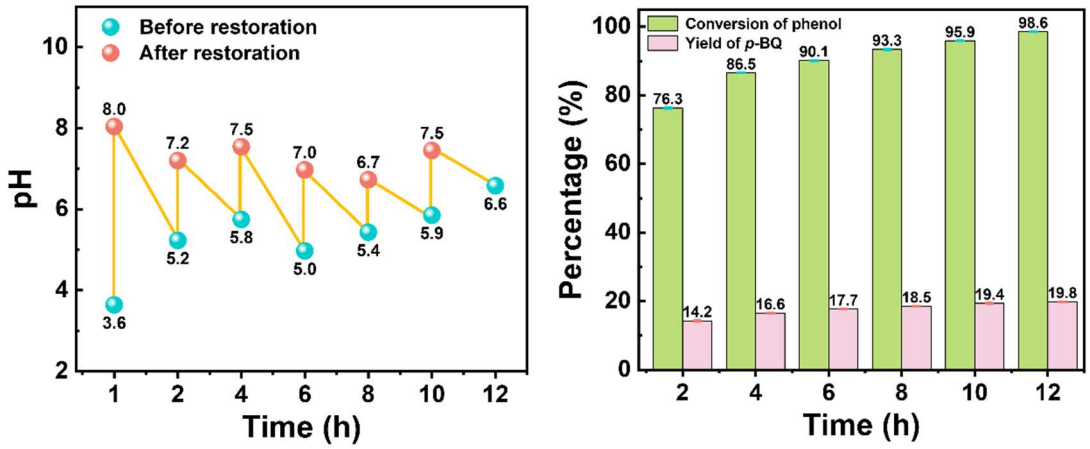

Figure S18. The ECO performance by the Co-Mn(OH)2/NF electrode at 0.9 V during the 12h long-term measurements with periodic pH restoration.

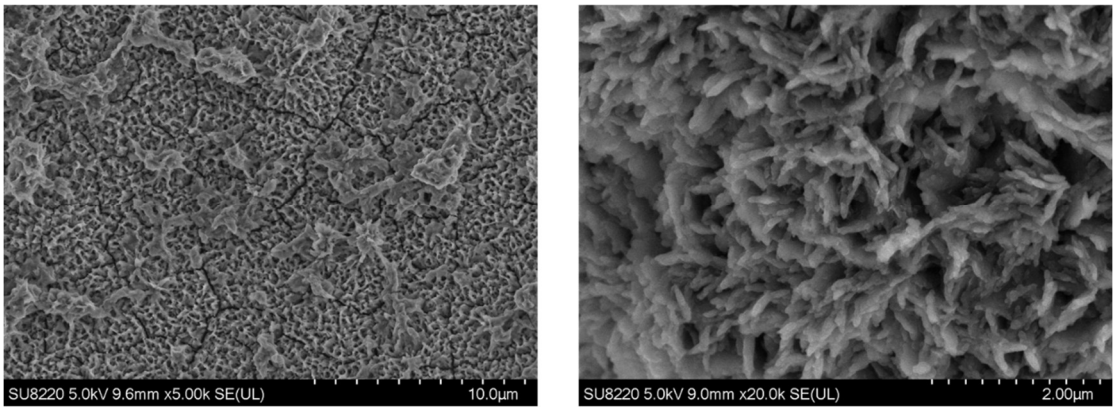

Figure S19. SEM images of the Co-Mn$(OH)_2$/NF after the prolonged ECO test.

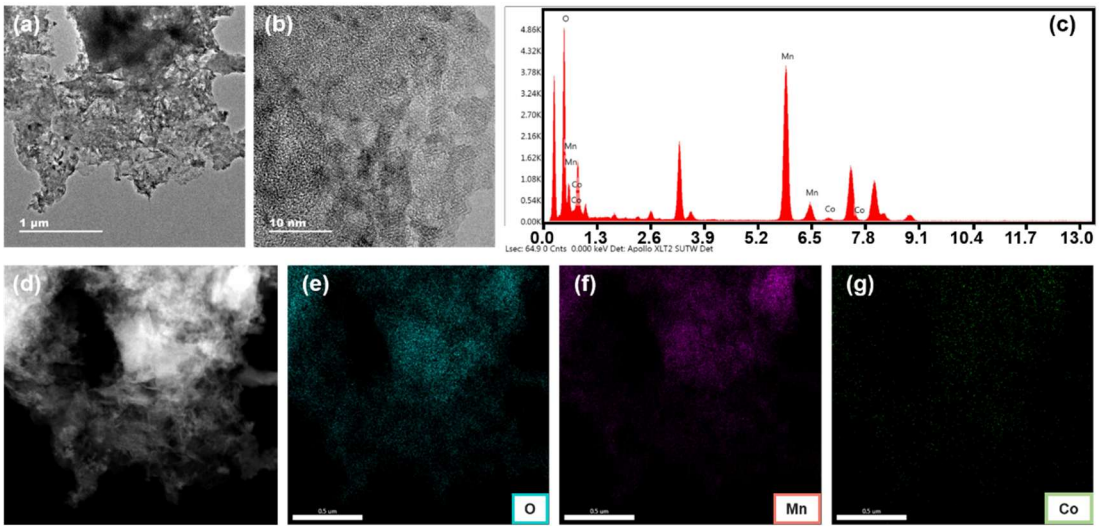

Figure S20. The (a) TEM image, (b) HR-TEM image, (c) EDX spectrum and (d-g) HAADF-STEM image and the corresponding elemental mapping images of the Co-$Mn(OH)_2$/NF after the prolonged ECO test.

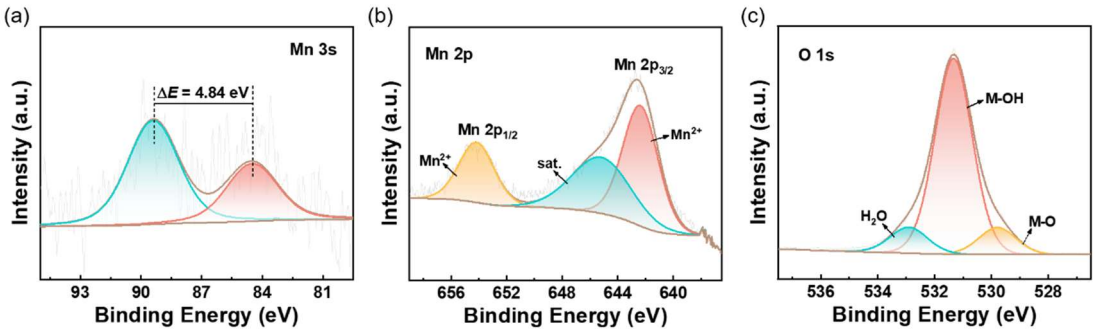

Figure S21. High-resolution XPS spectra for (a) Mn 3s, (b) Mn 2p and (c) O 1s of Co-$Mn(OH)_2$/NF after the prolonged ECO test.

^{1}H NMR (400 MHz, D_2O) δ 7.27 – 7.21 (m, 17H), 6.91 (t, *J* = 7.4 Hz, 8H), 6.84 (d, *J* = 7.7 Hz, 17H), 6.75 (s, 4H).

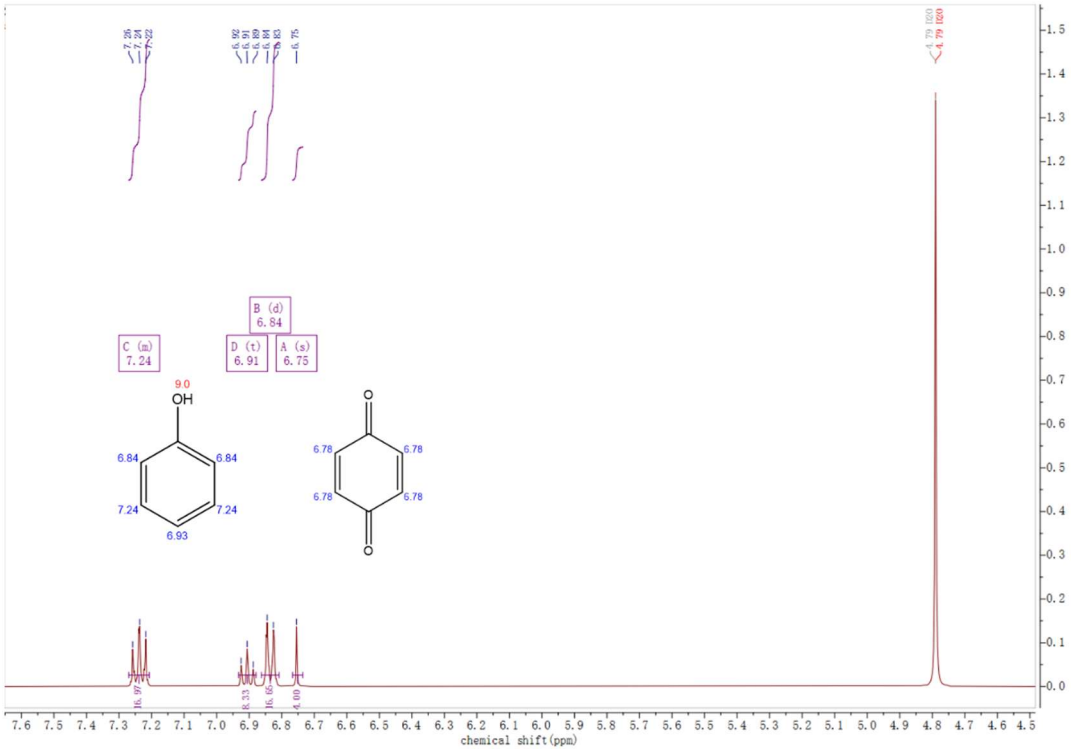

Figure S22. ^{1}H NMR results for the produced *p*-BQ.

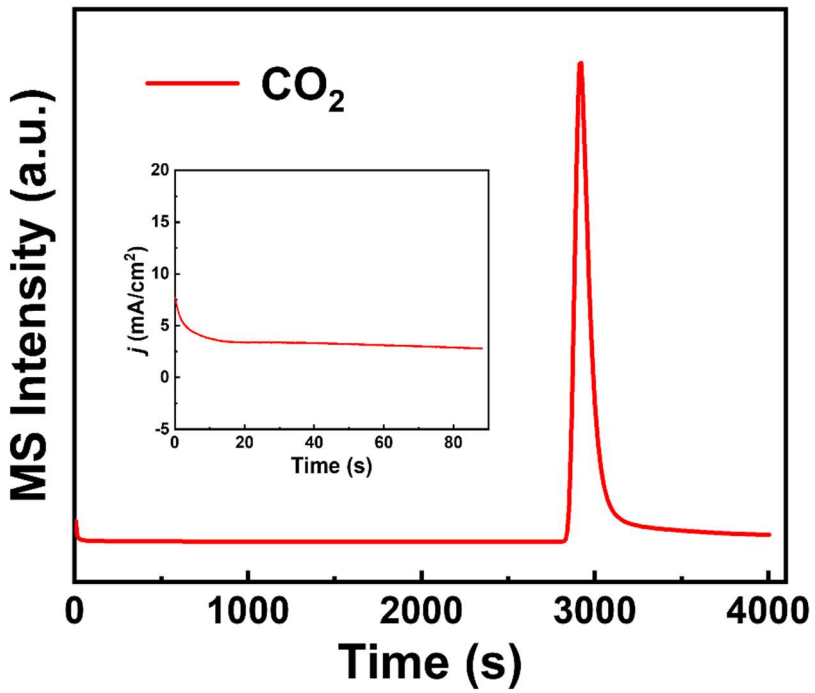

Figure S23. In-situ DEMS monitoring of gaseous products during phenol electrooxidation on Co-$Mn(OH)_2$/NF.

Table S1. ICP-OES results for Co-$Mn(OH)_2$/NF.

The starting molar ratio of Co to Mn	Catalysts	Co (wt%)	Mn (wt%)	The deposited molar ratio of Co to Mn
1:100	Co-$Mn(OH)_2$	0.60	46.55	1.02:85.75